JOURNAL OF APPLIED ELECTROCHEMISTRY 7 (1977) 517–530

Kinetics and mechanism for the hydrothermal decomposition of sodium amalgam promoted on graphite electrodes containing iron

R. L. DOTSON,* A. JENKINS†

* *Olin Chemicals Group, Charleston Technology Center, P.O. Box 248, Charleston, Tenn. 37310, USA*
† *Chemical Engineering Department, Clemson University, Clemson, S. C. 29631, USA*

Received 4 January 1977

The kinetics for the hydrothermal decomposition of sodium amalgam was studied in the presence of water and caustic soda on graphite electrodes containing iron.

Regression analysis of over 1000 data points in a linear regression analysis yielded the following rate expression, explaining 89% of the variance in the data, leaving 11% of the variance unexplained:

$$r = -\mathrm{d(Na)/dt} = 187{\cdot}8\,(T)^{-2/3} \exp(-196{\cdot}9/RT)\,(\mathrm{Na})^{3/4}\,(\mathrm{NaOH})^{-1/5}.$$

The decomposition rate of sodium amalgam is strongly limited by the rate of diffusion of sodium metal atoms in the mercury, and also the activity of water at the active cathodic sites on the catalyst. The activation energy for charge transfer for this process is low at 196·9 cal mol^{-1} or 8·5 mV.

The range of variables studied was: temperature – 25, 50 and 85° C; caustic concentration – 10, 30 and 50 wt.%; amalgam concentration – 0·1, 0·2 and 0·3 mol.%, and finally with iron concentrations in the graphite matrix of – 215·9, 929·5 and 6180 ppm.

List of symbols

R	1·987 cal $(\mathrm{K\,mol})^{-1}$ = ideal gas law constant.
$\bar{R}$	*M–M* distance between nearest neighbours in the crystal lattice of the electrode used to calculate the Madelung constant.
r	$i/nF = -\mathrm{d(Na)/d}t$ = reaction rate giving loss of amalgam in mol min^{-1}.
T	(273 + ° C) = absolute temperature (K).
(Na)	C_{Na} = $\mathrm{mol\,l}^{-1}$ = concentration of sodium in mercury.
(NaOH)	C_{NaOH} = $\mathrm{mol\,l}^{-1}$ = concentration of sodium hydroxide in water solution.
Z^+, Z^-	charges on cation and anion, respectively.
(M)	active centre on the iron promoter catalyst.
i	total net current density.
i_+	anode partial current density.
i_-	cathode partial current density.
i_0	exchange current density, at $i_+ = i_- = i_0$, where $\eta \to 0$, and the mutually compensating anodic and cathodic current densities are present at the equilibrium potential.
η	overpotential on the electrode, $E - E^0$.
A	Arrhenius coefficient, constant.
D_{Na^0}	diffusion coefficient of sodium metal in mercury in $\mathrm{cm}^2\,\mathrm{min}^{-1}$.
$\bar{K}$	rate constant, temperature and activation energy dependent.
k	rate constant, independent of temperature and activation energy.
a_{Na}	(Na) = C_{Na} = activity of sodium in mercury and to a good approximation equal to its concentration.
a_{w}	activity of water in presence of caustic.
x	distance normal to the catalyst surface (cm).
$\mathrm{d}x$	change in distance normal to the catalyst surface.
t	time at which sample is collected and reaction is quenched.

t_0	initial time zero.
a, b	the order of the reaction, or the exponential power to which the concentration is raised, as opposed to the molecularity of the reaction, or the molecules/collision. The order is empirical and the molecularity is theoretical.
Y	$\ln(-\mathrm{d}[\mathrm{Na}]/\mathrm{d}t) = \ln k + n\ln T + E_a/RT + a\ln(\mathrm{Na}) + b\ln(\mathrm{NaOH})$, the linear least squares curve fitting program equation.
$B_{0,1,2,3,4}$	coefficients for the linear least squares curve fitting program.
x_i	sample measurement i.
d	$x_i - \bar{X}$ = deviation from the average.
σ	standard deviation, $\sqrt{\Sigma d^2/\bar{n}}$.
σ^2	variance, or the mean squared deviation from the mean, $\Sigma d^2/\bar{n}$.
$\bar{X}$	arithmetic mean, $x_1 + x_2 + \ldots x_n/\bar{n}$
$\bar{n}$	total number of measurements.

1. Introduction

The decomposition of sodium amalgam by an aqueous caustic solution is greatly accelerated by contacting it with localized anodic centres on graphite formed where a metal catalyst is used as the activator at the boundary surface. A three-phase region of contact of water, sodium amalgam, graphite, contact catalyst and atomic hydrogen must be maintained in the active site region in order for the amalgam decomposition reaction to proceed at an appreciable rate.

Little is known at present about the active centres on catalysts at solid surfaces, because of the difficulty in reproducing identical batches of solid catalysts. Regions of high and low surface activity are known to correspond with differences in intrinsic atomic composition, space group symmetry and surface morphology, etc., at the given catalytic surface. Correlations of surface geometry with catalytic activity are just coming under careful study [1, 2].

The active areas on the surface of graphite electrodes form local cells where the amalgam acts as an anode and the substrate material as the cathode in a galvanic cell directly shorted according to the couple shown here in a medium of caustic and water:

$$\mathrm{NaHg}_x\,[\mathrm{NaOH(aq)}\,(M)]\,\mathrm{H}_2. \qquad (1)$$

During this process a positive electric current flows from the sodium atoms in the mercury to the carbon atoms in the graphite, through the external circuit, and discharges at the active centre (M) on the iron cathode. The reaction rate is equal to the total flux of sodium ions moving away from the surface of the mercury, as shown in the diffusion equation:

$$r = i/nF$$
$$= -C_{\mathrm{Na^o}}C_{\mathrm{H_2O}}D_{\mathrm{Na^o}}\bar{K}(\mathrm{d}\ln a_{\mathrm{Na^o}}/\mathrm{d}x)(\mathrm{d}\ln a_{\mathrm{w}}/\mathrm{d}x) \qquad (2)$$

where $C_{\mathrm{Na^o}}$ is the bulk concentration of sodium atoms in the mercury and $C_{\mathrm{H_2O}}$ the concentration of water at the cathode in mol cm^{-3} [3, 4].

2. Experimental

Experiments were carried out on samples of graphite decomposer packing from the Union Carbide Corporation having iron concentrations of 215·9, 929·5 and 6180 ppm. Caustic concentrations of 10, 30 and 50 wt.% and sodium amalgam concentrations of 0·1, 0·2 and 0·3 mol.% were studied at temperatures of 26, 51 and 85° C.

The laboratory test method used to determine the activity of packing for sodium amalgam decomposition involved drilling a 3/8 × 1/2 in. deep hole into the graphite sample, immersing it as a cup into the given caustic solution and bringing it to temperature. At t_0, a weighed amount of known strength amalgam was poured into the hole in the sample cup through a Teflon tube, as shown in Fig. 1. The amalgam was then allowed to react for a time t, with the net reaction time measured on an electric timer. At time t, the amalgam was dumped into a separatory funnel containing 100 ml of acetone to remove the water from the reaction and to arrest it. The amalgam was subsequently placed into a gas buret containing 15 wt.% hydrochloric acid and the mol.% sodium remaining determined from the amount of hydrogen evolved, as seen in Fig. 1. The experiment was then repeated at increasing time intervals until the reaction of sodium in the mercury was complete.

a. gas buret
b. buret containing amalgam
c. electric timer
d. bottles containing weighed amount of amalgam
e. constant temperature bath
f. graphite sample containing amalgam
g. teflon tubing to graphite sample
h. graduated cylinder containing caustic

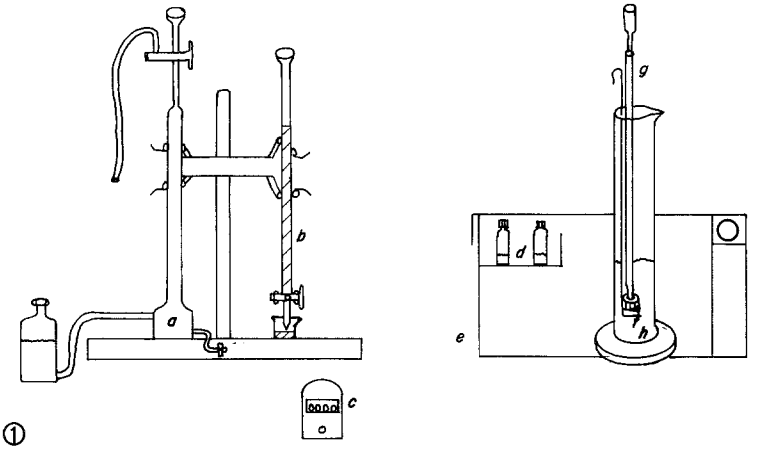

①

Fig. 1. Experimental apparatus, gas buret and graphite sample cup assembly used to determine the concentration–time data for the sodium amalgam decomposition.

3. Results and discussion

3.1 *Kinetics*

The rate of decomposition of sodium amalgam is related directly to the current flow from the amalgam to the anodically active site on the graphite matrix. Graphite is essential for the decomposition, since the reaction does not take place in the presence of 40% iron bound into a solid matrix without graphite. The rate of amalgam decomposition is also regulated by the intrinsic cathodic overpotential, ohmic electrolyte losses, packing resistance losses, amalgam concentration and water activity, contact resistance and finally to the reaction temperature.

The fundamental objective of this reaction rate study was to develop a convenient method for recording the instantaneous sodium metal concentration in the amalgam at specified time intervals, and then develop a rate equation from the data. The experimental collection of concentration–time data in these runs utilized a simple, direct method of standard chemical analysis. It produced the curves shown in Figs. 2(a–c), 3(a–c) and finally 4(a–c), where the fraction of sodium metal remaining at any time t, is plotted at the various temperatures, caustic concentrations, initial amalgam strengths and iron concentrations. Most of the data yielded less than 2% standard deviation for ten identical runs.

These experimental runs were made up of nine data sets, each one having three complete runs in it. Fig. 2 gives the data shown for 10% caustic; Fig. 3 at 30% and Fig. 4 at 50% caustic with 0·3, 0·2 and 0·1 mol.% initial sodium concentration, at 25, 50 and 85° C, and 215·9, 929·5 and finally 6180 ppm iron content.

This work is very significant as it relates to mercury cell operation in a working plant [5–8]. Highly active denuder packing in a cell will produce higher concentrations of caustic and require shorter hold-up times for the amalgam in the denuder. These studies provide fundamental kinetic and mechanistic data and information for the decomposition of sodium amalgam in alkaline solutions as a function of temperature and the concentration of caustic and amalgam. The decompositions were carried out on graphite with different concentrations of iron in and on its surface. After completing the laboratory studies, an analysis of the data produced a rate equation using a least squares computer regression analysis program.

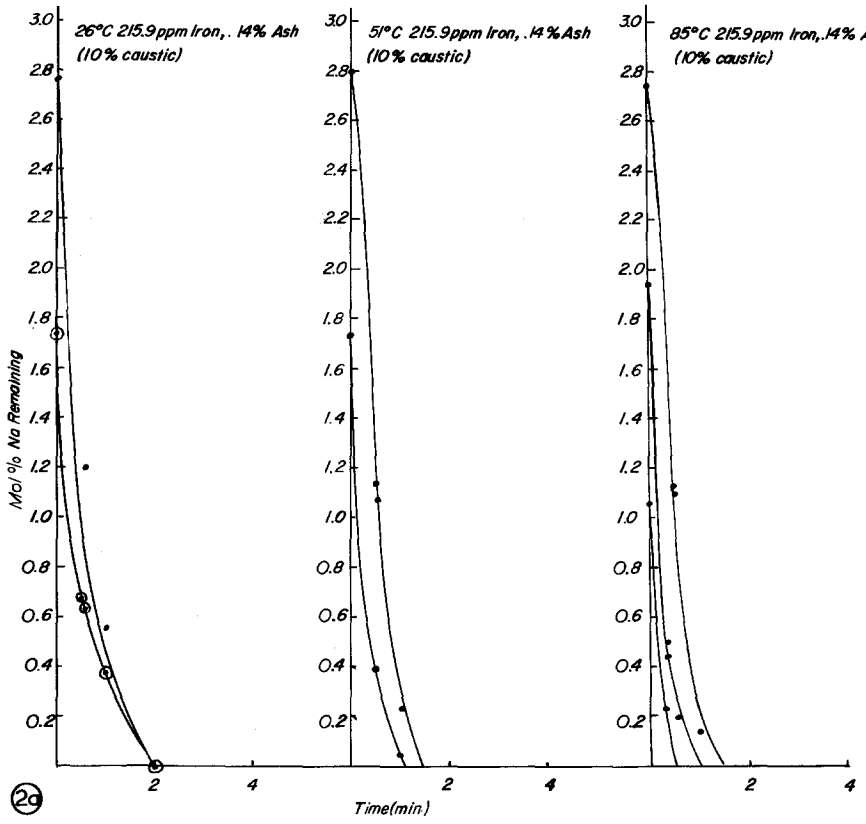
26°C 215.9ppm Iron, .14% Ash (10% caustic)
51°C 215.9ppm Iron, .14% Ash (10% caustic)
85°C 215.9ppm Iron, .14% Ash (10% caustic)
Mol % Na Remaining
Time(min)

(2a)

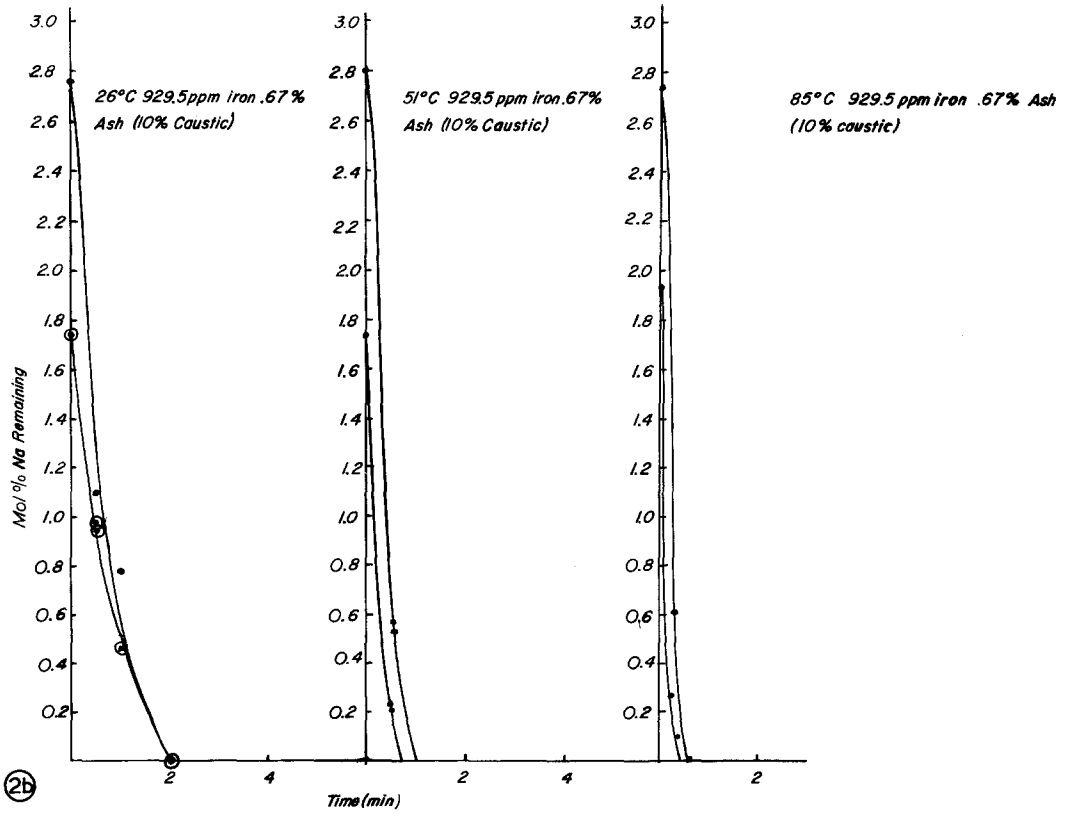
26°C 929.5ppm iron .67% Ash (10% Caustic)
51°C 929.5 ppm iron .67% Ash (10% Caustic)
85°C 929.5 ppm iron .67% Ash (10% caustic)
Mol % Na Remaining
Time (min)

(2b)

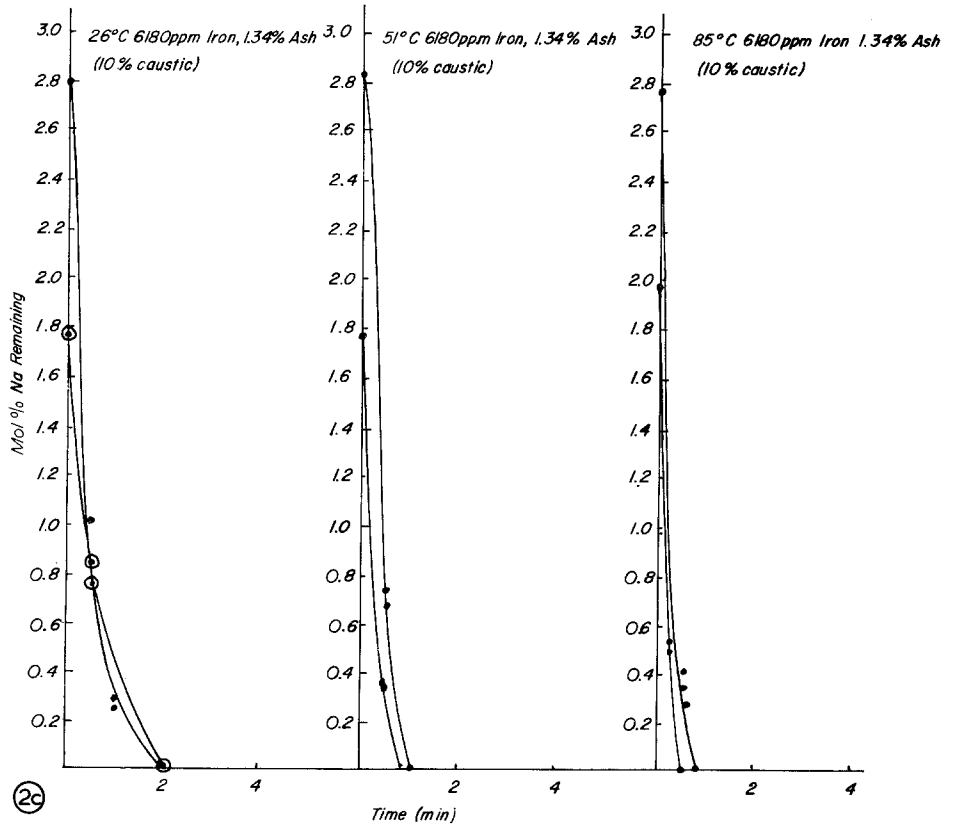

Fig. 2(a). Comparison of amalgam decomposition rates on graphite with 215·9 ppm iron content, showing the effect of amalgam concentration and temperature at 10% caustic.

Fig. 2(b). Comparison of amalgam decomposition rates on graphite with 929·5 ppm iron content, showing the effect of amalgam concentration and temperature at 10% caustic.

Fig. 2(c). Comparison of amalgam decomposition rates on graphite with 6180 ppm iron content, showing the effect of amalgam concentration and temperature at 10% caustic.

The following two-step catalytic sequence is suggested from the data analysis:

$$Na^{o} + S_1 \longrightarrow Na^{+} + S_1 - [e^{-}] \quad (3)$$

$$S_1 - [e^{-}] + S_2 \longrightarrow S_1 + S_2 - [e^{-}] \quad (4)$$

$$S_2 - [e^{-}] + H_2O \longrightarrow S_2 - H + OH^{-} \quad (5)$$

$$S_2 - H + S_2 - H \longrightarrow H_2(g) + 2S_2. \quad (6)$$

Two main steps that are seen in Reactions 3 and 5, the rate limiting step in 3 and the recombination reaction in 6. The anodic and cathodic active centres on the packing are denoted here as S_1 and S_2, respectively [9–11].

The overall reaction rate can be written in general terms as follows:

$$r = -\mathrm{d}(Na^{o})/\mathrm{d}t = \mathrm{f}[\bar{K}, C_{Na^{o}}, C_{NaOH}] \quad (7)$$

thus,

$$-\mathrm{d}(C_{Na^{o}})/\mathrm{d}t = \bar{K}\, C^{a}_{Na^{o}}\, C^{b}_{NaOH} \quad (8)$$

and then letting, $C_{Na^{o}} = Na$, and also $C_{NaOH} = NaOH$, then taking the logarithms of both sides of Equation 8 gives:

$$\log [-\mathrm{d(Na)}/\mathrm{d}t] = \log \bar{K} + a\log (Na) + b\log (NaOH) \quad (9)$$

now putting in the Arrhenius relationship,

$$\bar{K} = A\exp (E_a/RT) \quad (10)$$

so that,

$$\log [\bar{K}] = \log A + E_a/RT \quad (11)$$

and finally,

$$\log [-\mathrm{d\,(Na)}/\mathrm{d}t] =$$

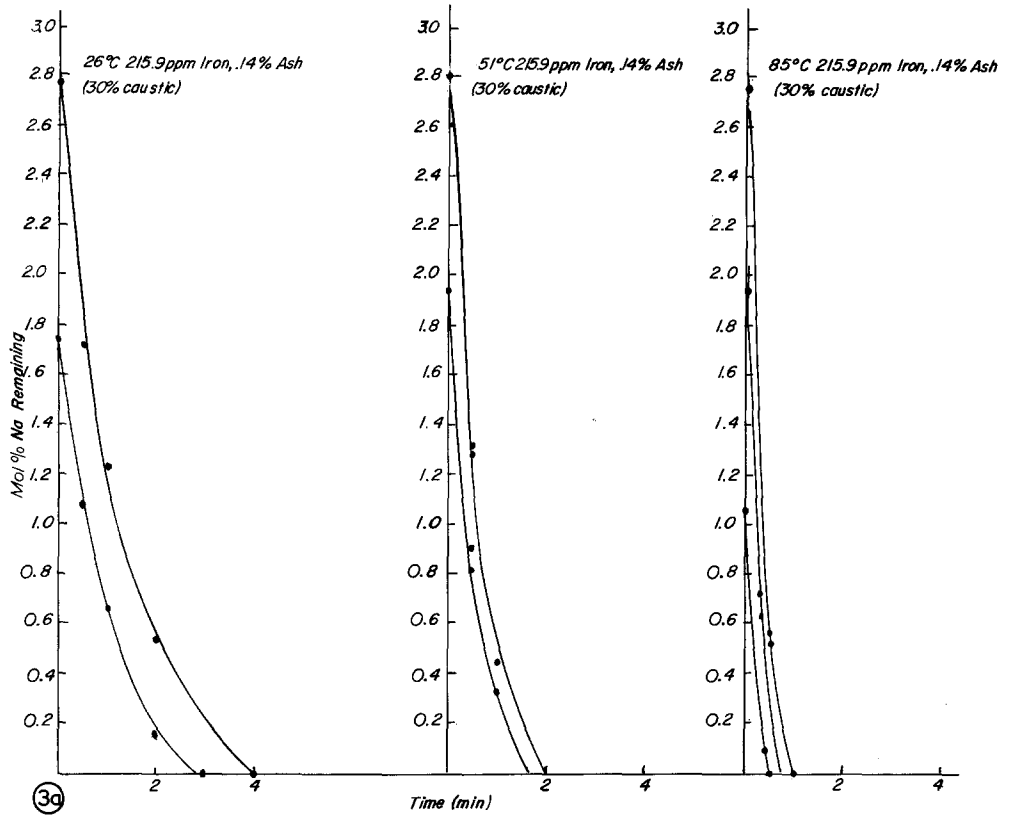
26°C 215.9ppm Iron, .14% Ash
(30% caustic)
51°C 215.9ppm Iron, .14% Ash
(30% caustic)
85°C 215.9ppm Iron, .14% Ash
(30% caustic)
Mol % Na Remaining
Time (min)

(3a)

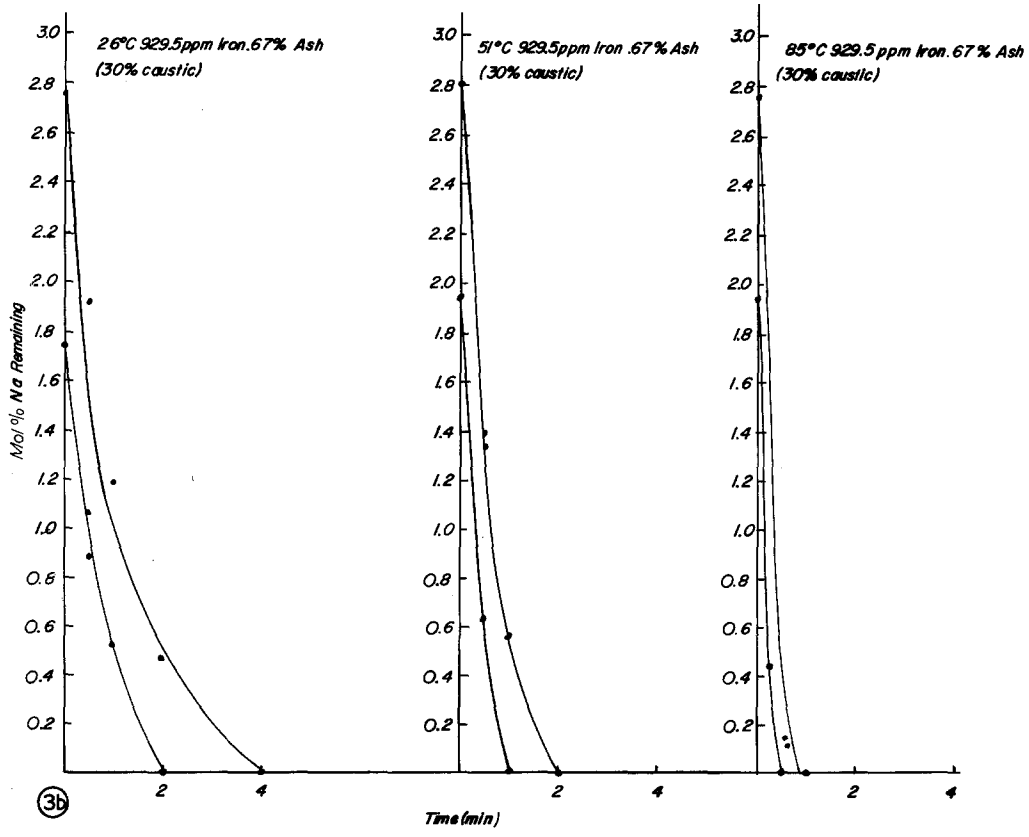
26°C 929.5ppm Iron .67% Ash
(30% caustic)
51°C 929.5ppm Iron .67% Ash
(30% caustic)
85°C 929.5ppm Iron .67% Ash
(30% caustic)
Mol % Na Remaining
Time (min)

(3b)

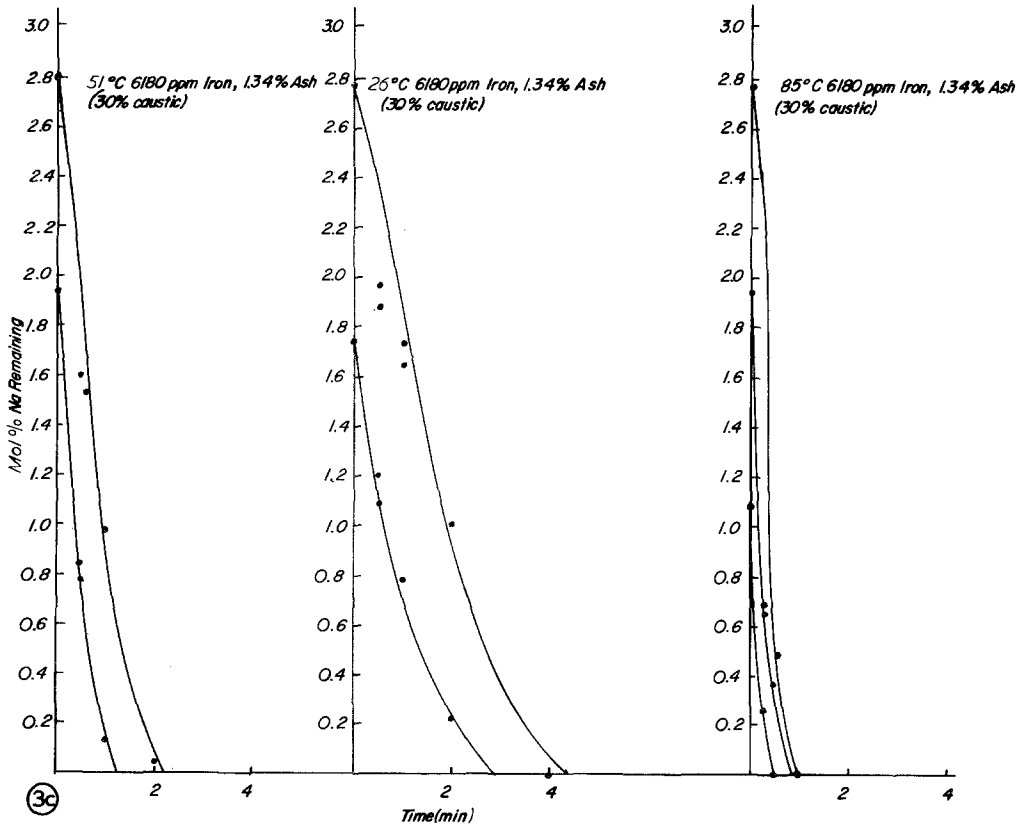

Fig. 3(a). Comparison of amalgam decomposition rates on graphite with 215·9 ppm iron content, showing the effect of amalgam concentration and temperature at 30% caustic.

Fig. 3(b). Comparison of amalgam decomposition rates on graphite with 929·5 ppm iron content, showing the effect of amalgam concentration and temperature at 30% caustic.

Fig. 3(c). Comparison of amalgam decomposition rates on graphite with 6180 ppm iron content, showing the effect of amalgam concentration and temperature at 30% caustic.

$$= [\log A + E_a/RT] + a\log(\mathrm{Na}) + b\log(\mathrm{NaOH}) \quad (12)$$

where,

$$\log[A] = \log k + n\log T \quad (13)$$

so that,

$$\log[-\mathrm{d(Na)}/\mathrm{d}t] = [\log k + n\log T] + E_a/RT + a\log(\mathrm{Na})\, b\log(\mathrm{NaOH}) \quad (14)$$

is now in a convenient linear form for the regression analysis [12–15],

$$Y = B_0 + B_1X_1 + B_2X_2 + B_3X_3 + B_4X_4. \quad (15)$$

Over 1000 data points were fed into the linear regression analysis program, Equation 15, and the computer program generated the following rate equation:

$$r = -\mathrm{d(Na)}/\mathrm{d}t = 187{\cdot}8\,(T)^{-2/3} \times \exp(-196{\cdot}9/RT)\,(\mathrm{Na})^{3/4}\,(\mathrm{NaOH})^{-1/5} \quad (16)$$

which explains 89% of the variance in the data, σ^2, leaving 11% of the variance unexplained by either the goodness-of-fit of Equation 16, to the data or to the probable errors in precision and accuracy of the data. The variance is an excellent measure of the uncertainty in the fit of the data to the mean.

The concentration of the caustic can now be written in terms of the specific water activity, a_w,

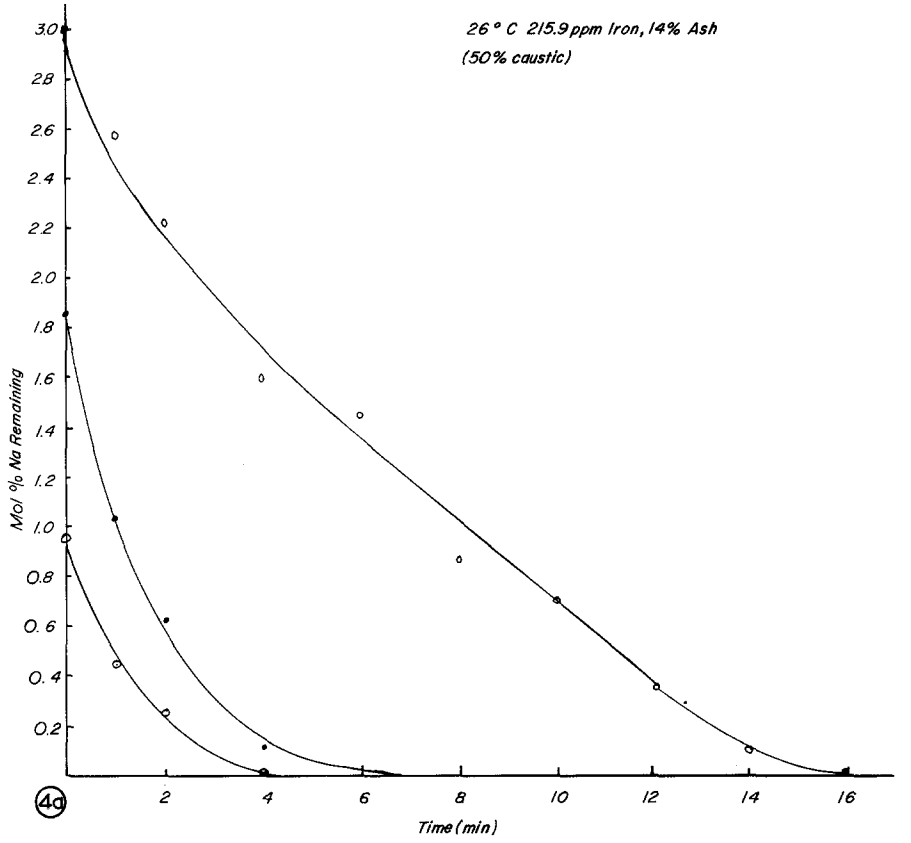
26° C 215.9 ppm Iron, 14% Ash
(50% caustic)
Mol % Na Remaining
Time (min)
4a

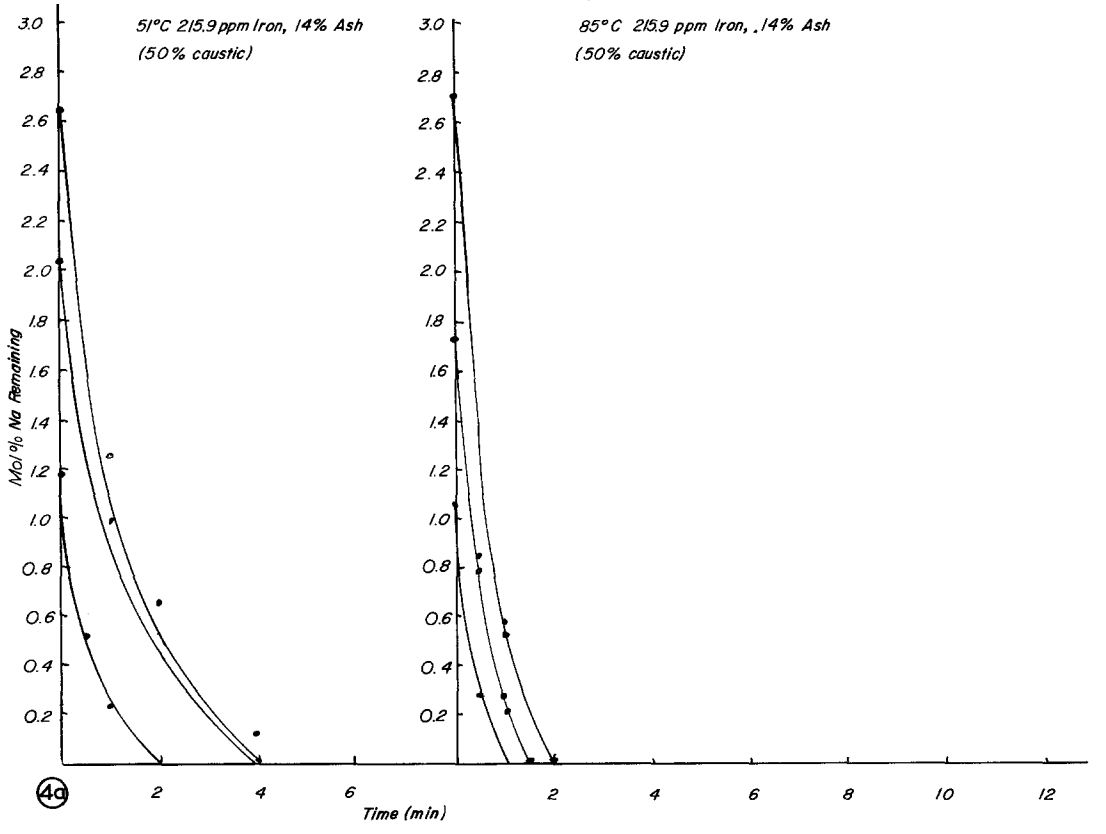
51°C 215.9 ppm Iron, 14% Ash
(50% caustic)
85°C 215.9 ppm Iron, 14% Ash
(50% caustic)
Mol % Na Remaining
Time (min)
4a

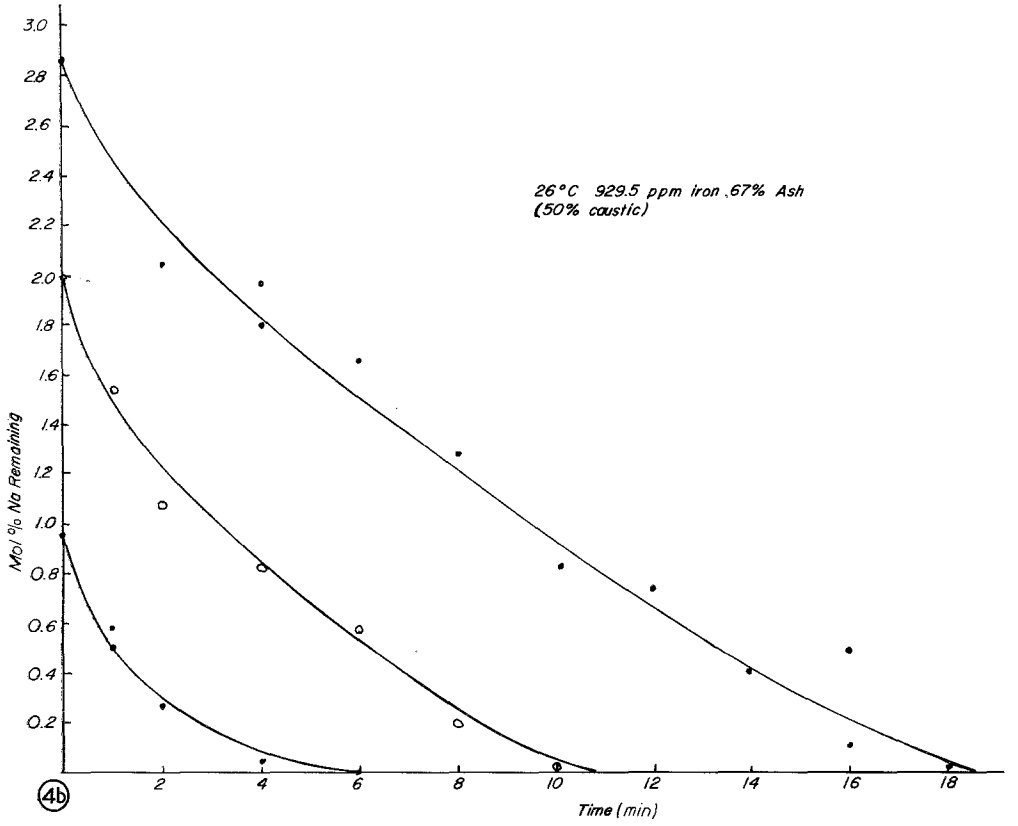
26°C 929.5 ppm iron .67% Ash
(50% caustic)
Mol % Na Remaining
Time (min)
4b

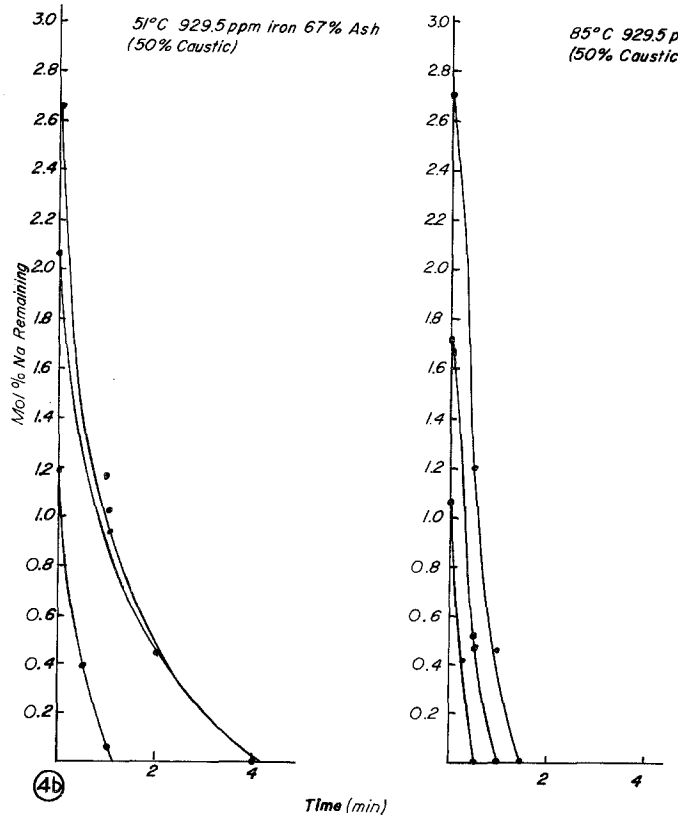
51°C 929.5 ppm iron 67% Ash
(50% Caustic)
85°C 929.5 ppm iron .67% Ash
(50% Caustic)
Mol % Na Remaining
Time (min)
4b

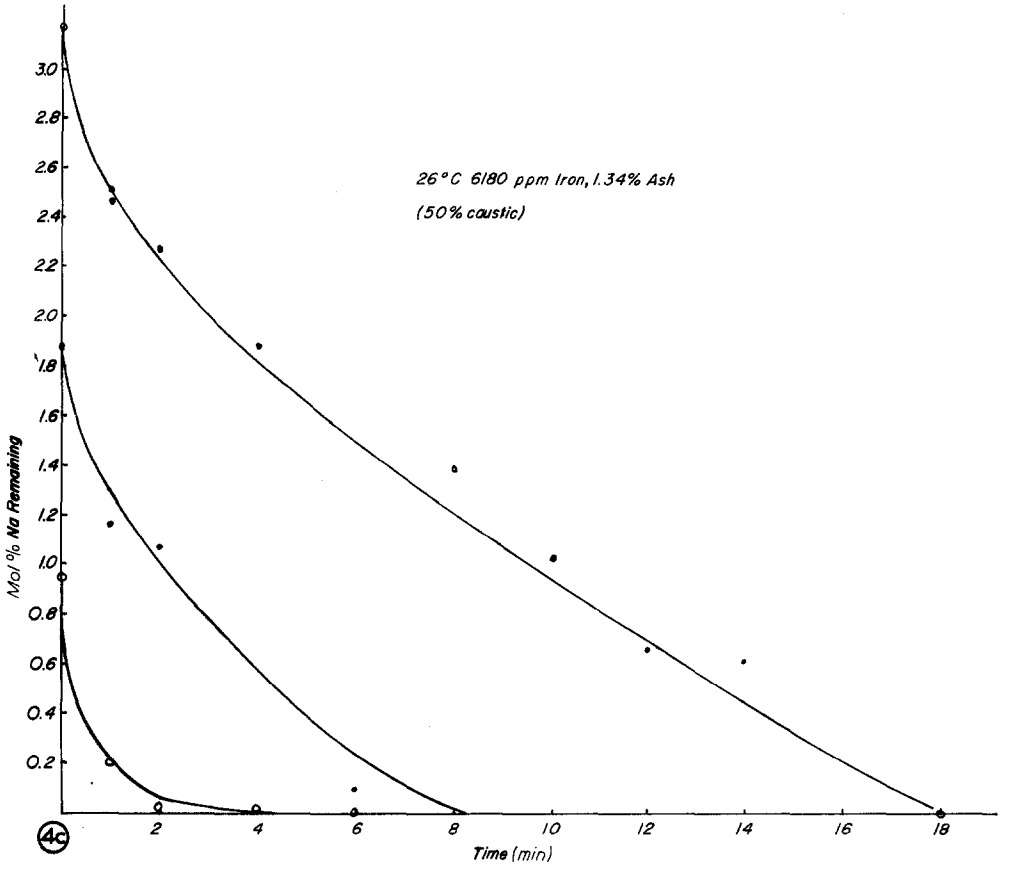
26°C 6180 ppm Iron, 1.34% Ash
(50% caustic)
Mol % Na Remaining
Time (min)
Ac

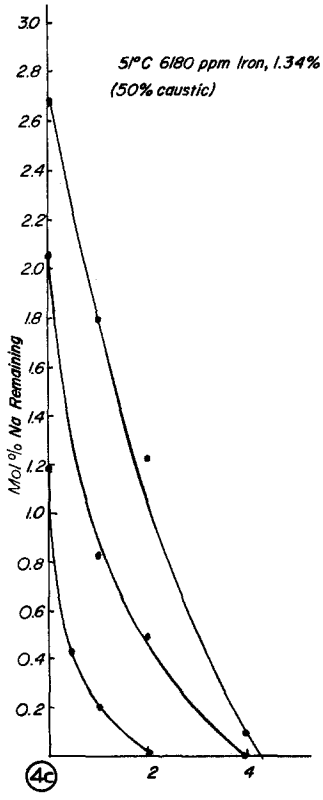
51°C 6180 ppm Iron, 1.34% Ash
(50% caustic)
Mol % Na Remaining
Ac

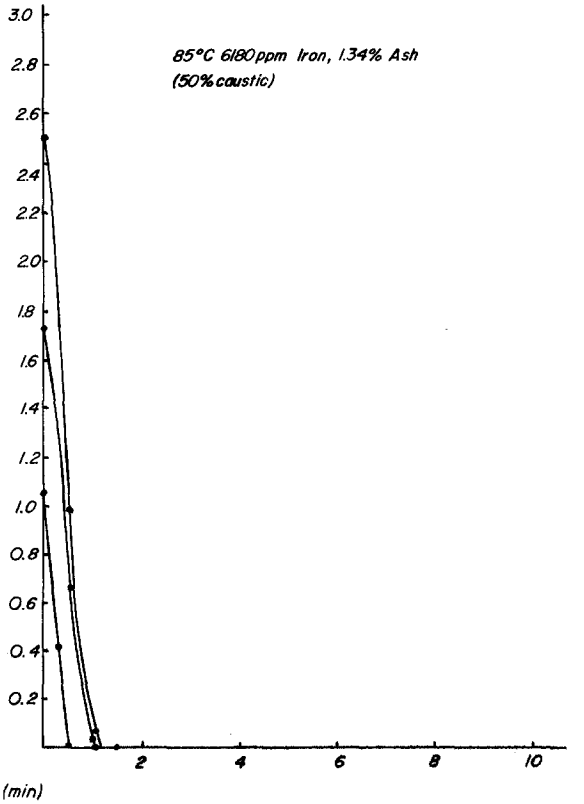
85°C 6180ppm Iron, 1.34% Ash
(50% caustic)
Time (min)

using the data in Table 1 [16–22], and the linear equation:

$$(\text{NaOH}) = 21{\cdot}28 - 21{\cdot}324\,(a_w). \quad (17)$$

Equation 16 establishes a standard, general kinetic relationship for defining and quantifying the terms that control the rate of amalgam decomposition on graphite, where the concentration of iron does not effect the rate significantly in the ranges studied [16–22].

3.2 *Mechanism*

The goal of this kinetic investigation is to define the reaction mechanism, resolve the overall reaction into component steps, and then determine the corresponding partial rates. Reactions having rates that are controlled by mass transport, such as the anodic discharge of mercury amalgam, remove reactants as a function of time and thus have the effect of overlapping the true phase transition reactions that can occur, that is where the amalgamated sodium metal in the sodium–mercury alloy changes to aggregated clusters.

The standard techniques of volumetric and gravimetric chemical analyses used in this study provide rate information of a direct nature as opposed to the galvanostatic and potentiostatic methods. The latter techniques require the neglect of concentration overpotential and the determination of diffusion patterns near to the electrode in order to obtain meaningful relationships such as Equation 16 [23].

Table 1. Molal concentrations of caustic, M NaOH, with corresponding water activities, a_w [16–22]

Wt.% NaOH	*M NaOH*	a_w
5·54	1·465	0·95
9·83	2·726	0·90
13·32	3·840	0·85
16·10	4·798	0·80
20·00	6·565	0·70
24·70	8·183	0·60
28·15	9·792	0·50
31·58	11·54	0·40
35·29	13·63	0·30
40·00	16·67	0·20
48·00	23·05	0·10

Equation 16 shows that the activation energy for charge transfer is very low,

$$0{\cdot}1969\ \text{kcal}/23{\cdot}06\ \text{kcal/V mol} = 8{\cdot}54\ \text{mV}$$

and since the activation energy is directly proportional to overpotential in this case, where at 118·4 mV the reverse current is 1% of the total, at 59·2 mV the reverse current is 10% of the total. This means that at 8·5 mV,

$$i_+/i_- = -\exp\,(F/RT[0{\cdot}0085]) \quad (19)$$

and,

$$i_+ = 1{\cdot}391\,(i_-),$$

or that the reverse current, i_-, is 42% of the total current and that the quantum mechanical transfer of electrons through the metal/electrolyte interface is very close to equilibrium and not significant in limiting the rate of decomposition of sodium amalgam in the ranges of iron concentration studied [24–28]. The iron at the cathodic site on the graphite substrate is thus residing at the experimental, 'Pourbaix', boundary between the domains of corrosion, immunity and passivation as noted by the following reduction potentials related to the basic solution conditions [29, 30]:

$$2e^- + 2H_2O \rightleftharpoons 2OH^- + H_2 - \overset{E^o}{0{\cdot}83}\ \text{V} \quad (20)$$

$$2e^- + Fe(OH)_2 \rightleftharpoons 2OH^- + Fe^o - 0{\cdot}88\ \text{V}. \quad (21)$$

Under the conditions observed from Equation 19, we can assume that,

$$i_+ = i_- = i_0,$$

Fig. 4(a). Comparison of amalgam decomposition rates on graphite with 215·9 ppm iron content, showing the effect of amalgam concentration and temperature at 50% caustic.

Fig. 4(b). Comparison of amalgam decomposition rates on graphite with 929·5 ppm iron content, showing the effect of amalgam concentration and temperature at 50% caustic.

Fig. 4(c). Comparison of amalgam decomposition rates on graphite with 6180 ppm iron content, showing the effect of amalgam concentration and temperature at 50% caustic.

at the cathodic sites, and therefore the dominance of the exchange current density shows that the reaction is controlled by mass transfer at the anodic site, and not by the charge transfer at the cathodic site, as seen in Fig. 5. Based on thermodynamic considerations, the more negative the reduction potentials in Reactions 20 and 21, the greater is the tendency of the reactions to take place, so that both will occur under the conditions encountered in a normal mercury cell denuder under load.

The prime limitation of the reaction rate is slow diffusion of sodium metal to the surface of the alloy droplet. This is in good agreement with the conclusions of previous workers [29, 30]. Since the majority of the experimental data was taken at sodium amalgam concentrations below 1%, the region which Rousar *et al.* [3] have studied also demonstrates that diffusion is rate-controlling. The conclusions reached here should, however, not be extended beyond the 1% sodium concentration level in the amalgam.

The rate limiting step at the cathodic site of the packing, in alkaline solution, is the transfer of a proton from a water molecule. At this site, the fundamental charge transfer control mechanism involves the region of solution next to the electrode as well as the surface structure of the solid phase [29, 30].

One or more polymorphic forms of iron oxides can exist at a cathodic surface where three dimensional crystalline compounds are produced to give a zone of high anisotropy in the solid state, as shown in Fig. 5.

The relationship of activity to surface oxidation and bonding of the iron to the graphite substrate is an area subject to further extensive research.

The nature of an electrode surface is the key factor in facilitating electron transfer processes. Oxide layers can be used to carry out electrochemical oxidation and reduction reactions with a current passing through the electrode and used to replenish the surface oxides. These oxides form in the surface monolayers on the metal substrate, which can be in a partially reduced state to enhance the reaction.

The reactive combination of metal, iron, graphite and oxygen can occur. The reaction of the metal surface with oxygen from water, or air, yields non-ordered two dimensional structures. Oxygen has a strong tendency to form disordered surface films of oxide ions. If a surface becomes cleaved along the (111) plane, as shown in view A–A of Fig. 5, the structure that is obtained becomes a simple extension of the substrate. The single electron left above each atom of the top layer of atoms is according to bond theory energetically unstable, and charge transfer readily occurs there to produce alternate positive and negative ions by some first-order reconstructive transitions that provide a more stable bonding arrangement.

The electronic properties are a major factor in affecting catalysis. If a metal substrate is readily polarizable so that a balancing of positive charges forms under the negative surface ion and negative charge below the positive surface ions, the surface

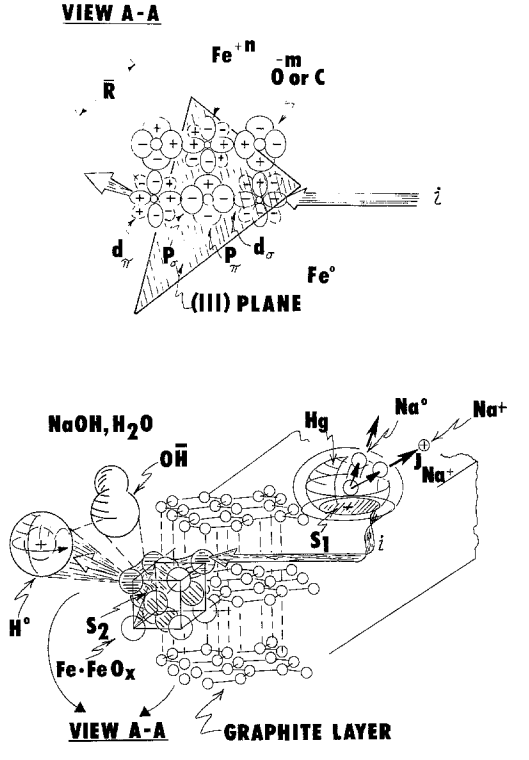

Fig. 5. Mechanistic model proposed for the charge and mass transfer in the active area of the iron–graphite amalgam local cell. The reaction is shown here to be controlled strongly by mass transfer of sodium atoms from the amalgam and only slightly by the charge transfer at the iron cathode. View A–A. shows the (111) plane, and the metal-oxide–graphite interface where cathodic electron transfer takes place. This represents an oblique view of the crystallographic space group across S2 at the oxide–graphite interface.

structure is firmly bonded to the substrate and the resulting 'Madelung constant' for the outer molecular monolayers becomes closer to that of a three dimensional structure than expected [31–33].

A summation of the Coulomb terms for interaction energy yields a Madelung constant of 1·54 for the two-dimensional, or 2-D, square lattice ionic structure and 1·76 for the three-dimensional, 3-D, cubic lattice terms, as:

$$E_c(\text{3-D}) = -e^2/\bar{R}[6 - 12/\sqrt{2} + 8/\sqrt{3} - 6/2 + \ldots] = 1{\cdot}76$$

$$E_c(\text{2-D}) = -e^2/\bar{R}[4 - 4/\sqrt{2} - 4/2 + 8/\sqrt{5} + 4/3 + \ldots] = 1{\cdot}54,$$

where $\bar{R}$ is the distance of closest approach between positive centres. The excess Madelung constant values over 1·00 in each case are a rough measure of the energy favouring order. The relative stabilities of the 2-D and 3-D surface structured crystallites also depends critically upon other energy terms such as repulsion energy, dipole–dipole interactions, and finally corrections for covalent and metallic bonding character.

Clean metal surfaces are found experimentally to have a much higher surface energy than ionic crystals. In most cases, except for MgO, and systems similar to it, this difference favours the termination of the metal crystal by an ionic 2-D structure with a contribution toward stabilization of several thousand kcal mol^{-1}. This means that surface reconstruction processes that bring positive ions into the top layer of the metallic domain are highly favoured.

In the present system of graphite impregnated with small domains of iron, the interfacial iron is rapidly oxidized to produce a hydrous oxide or oxy-hydroxide at its surface in the presence of water, as FeO.OH. It is a compound intermediate between oxides and hydroxides having the empirical composition:

$$x\text{FeO}\cdot y\text{Fe}_2\text{O}_3\cdot z\text{H}_2\text{O}$$

with $y : x$ ranging from 1 to 3. It can also be formed by precipitating mixed solutions of ferrous and ferric chlorides with NaOH, or by boiling α-FeO.OH with alkali in the presence of oxygen.

These oxides form at the working region in the electrode interface in the presence of alkali and a source of oxygen, such as water, according to these following reactions, recalling that all metals are thermodynamically unstable with respect to their oxides, except gold:

$$\text{Fe}^{\circ} + x\text{H}_2\text{O} \xrightarrow{\text{Fast}} \text{FeO}_x + 2x\text{H}^{\bullet}$$

$$\text{FeO}_x + x\text{H}_2\text{O} \xrightarrow{\text{Fast}} \text{FeO}_x\cdot(\text{OH})_x + x\text{H}^{\bullet}$$

$$\text{FeO}_x\cdot(\text{OH})_x + xe^- \xrightarrow{\text{Fast}} \text{FeO}_x + x\text{OH}^-$$

$$\text{Fe}^0 + 2x\text{H}_2\text{O} + xe^- \quad \text{FeO}_x + 3x\text{H}^{\bullet} + x\text{OH}^-$$

while the reaction of reduction of this monolayer at the interface is slow and incomplete, thereby lowering the overpotential very substantially over the metallic form of the dynamic interface:

$$\text{FeO}_x\cdot(\text{OH})_y + 2x\text{H}^{\bullet} \xrightarrow{\text{Slow}} \text{Fe}^0 + x\text{H}_2\text{O} + y\text{OH}^-.$$

4. Summary and conclusions

This study defines the rate equation and mechanism for the hydrothermal decomposition reaction of sodium amalgam on an electrode system of iron and graphite.

The reaction rate is shown to be controlled by diffusion of the sodium atoms from the amalgam into the surrounding water solution of sodium hydroxide. The strongest factors influencing the rate of decomposition are temperature, amalgam concentration and the water activity at the anodically activated sites.

Previous literature shows that the power to which sodium metal concentration in mercury is raised is 1/2, but in the present work we define the empirically determined order for sodium atoms in the mercury to be 3/4 in the rate expression. It is found that the plot of the former data produces a slight curve with sodium concentration plotted to the 1/2 power versus time, which should now be rejected in favour of the sodium concentration to the 3/4 power versus time.

Acknowledgements

We are indebted to the Olin Chemicals Group of the Olin Corporation and extend a special thanks to Mr Walter J. Sakowski and Mr James M. Ford of

Olin for their generous consultation and technical support of this work.

References

[1] S. Ross, 'Chemistry and Physics of Interfaces', American Chemical Society Publications, Washington, D.C., 103–159, (1965).

[2] E. F. Caldin, 'Fast Reactions in Solution', Blackwell Scientific Publications, Oxford (1964) pp. 164–84.

[3] I. Rousar, S. Rajasekaran and J. Cezner, *J. Electrochem. Soc.* **121** (3) (1974) 336–44.

[4] J. Hostomsky, I. Rousar and V. Cezner, *Collect Czech Chem Commun.* **40**(2) (1975) 483–96.

[5] J. S. Sconce, 'Chlorine, Its Manufacture, Properties and Uses', Robert E. Krieger Publishing Company, Huntingdon, N.Y. (1972) p. 176.

[6] C. L. Mantell, 'Electrochemical Engineering', McGraw-Hill Book Company, N.Y. (1960).

[7] O. Levenspiel, 'Chemical Reaction Engineering', 2nd Edn, John Wiley and Sons, Inc. N.Y. (1972) 41–7.

[8] F. Hine, *Electrochem. Technol.* **2**(3–4) (1964) 79.

[9] G. M. Harris, 'Chemical Kinetics', D. C. Heath and Company, Boston, (1966) pp. 41–7.

[10] S. Glasstone, K. J. Laidler and H. Eyring, 'The Theory of Rate Processes', McGraw-Hill Book Co., Inc., N.Y. (1941) pp. 339–400.

[11] M. Boudart, 'Kinetics of Chemical Processes', Prentice Hall, Inc., Englewood Cliffs, N.J. (1968) pp. 187–207.

[12] A. A. Frost and R. G. Pearson, 'Kinetics and Mechanism', 4th Edn, John Wiley and Sons, Inc., (1965) pp. 103–9.

[13] M. Jaksic and I. M. Csonka, *Electrochem. Technol.* **4**(1–2) (1966) 49–56.

[14] F. Hine, S. Yoshizawa, J. Kushiro and N. Yokota, *J. Electrochem. Soc., Japan,* **28** (1960) E-6.

[15] W. T. Martin and E. Reissner, 'Elementary Differential Equations', Addison-Wesley Pub. Co., Inc. London (1961) 112–15.

[16] B. E. Conway and R. G. Barradas, 'Chemical Physics of Ionic Solutions', John Wiley and Sons, Inc., New York (1966).

[17] H. S. Harned and J. C. Hecker, *J. Amer. Chem. Soc.* **55** (1933) 4838.

[18] G. Akerlof and G. Kegeles, *ibid* **62** (1940) 620.

[19] H. S. Harned and B. B. Owen, 'The Physical Chemistry of Electrolytic Solutions', American Chemical Society, Reinhold, New York (1958).

[20] W. Volk, 'Applied Statistics for Engineers, McGraw-Hill Book Co., New York (1969) p. 149.

[21] W. J. Youden, 'Statistical Methods for Chemists', John Wiley & Sons, Inc., New York (1964).

[22] E. L. Crow, F. A. Davis and M. W. Maxfield, 'Statistics Manual', Dover Publications, Inc., New York (1960).

[23] V. T. Pustovit, *Zh. Prik. Khim.* **45**(11) (1972) 2435–41.

[24] K. J. Vetter, 'Electrochemical Kinetics', Academic Press, New York (1967) pp. 104, 157.

[25] M. M. Jaksic, D. R. Jovanovic and I. M. Csonka, *Electrochimica Acta.* **13** (1958) 2077–87.

[26] R. Burian, J. Sucharda and J. Bale, *Chem.-Ing.-Techn.* **40** (1968) 18.

[27] M. Matusek and M. Franz, *Chem. Prum.* **24**(7–8) (1974) 370–7.

[28] F. Hine, F. Wang and K. Yamakawa, *Electrochim. Acta* **16** (1971) 1519–31.

[29] M. Pourbaix, 'Atlas of Electrochemical Equilibria in Aqueous Solutions', National Association of Corrosion Engineers, Houston, Texas (1974).

[30] E. Gileadi, E. Kirowa-Eisner and J. Pencinor, 'Interfacial Electrochemistry', Addison-Wesley Pub. Co., Reading, Mass. (1975).

[31] A. F. Wells, 'Structural Inorganic Chemistry', Clarendon Press, Oxford (1962).

[32] A. van der Ziel, 'Solid State Physical Electronics', Prentice-Hall, Inc., Englewood Cliffs, N.J. (1968).

[33] J. B. Goodenough, 'Metallic Oxides', Progress in Solid State Chem., Vol. 5, Pergamon Press, New York (1972).